Chemistry & Biology
Article

Structures of *Clostridium botulinum* Neurotoxin Serotype A Light Chain Complexed with Small-Molecule Inhibitors Highlight Active-Site Flexibility

Nicholas R. Silvaggi,[1] Grant E. Boldt,[2] Mark S. Hixon,[2] Jack P. Kennedy,[2] Saul Tzipori,[3] Kim D. Janda,[2] and Karen N. Allen[1,*]
[1] Department of Physiology and Biophysics, Boston University School of Medicine, Boston, MA 02118, USA
[2] Departments of Chemistry and Immunology, The Skaggs Institute for Chemical Biology, and Worm Institute of Research and Medicine (WIRM), The Scripps Research Institute, La Jolla, CA 92037, USA
[3] Division of Infectious Diseases, Tufts University School of Veterinary Medicine, North Grafton, MA 01536, USA
*Correspondence: allen@med-xtal.bu.edu
DOI 10.1016/j.chembiol.2007.03.014

SUMMARY

The potential for the use of *Clostridial* neurotoxins as bioweapons makes the development of small-molecule inhibitors of these deadly toxins a top priority. Recently, screening of a random hydroxamate library identified a small-molecule inhibitor of *C. botulinum* Neurotoxin Serotype A Light Chain (BoNT/A-LC), 4-chlorocinnamic hydroxamate, a derivative of which has been shown to have in vivo efficacy in mice and no toxicity. We describe the X-ray crystal structures of BoNT/A-LC in complexes with two potent small-molecule inhibitors. The structures of the enzyme with 4-chlorocinnamic hydroxamate or 2,4-dichlorocinnamic hydroxamate bound are compared to the structure of the enzyme complexed with L-arginine hydroxamate, an inhibitor with modest affinity. Taken together, this suite of structures provides surprising insights into the BoNT/A-LC active site, including unexpected conformational flexibility at the S1′ site that changes the electrostatic environment of the binding pocket. Information gained from these structures will inform the design and optimization of more effective small-molecule inhibitors of BoNT/A-LC.

INTRODUCTION

The neurotoxins produced by *Clostridium botulinum* (BoNTs), the most potent toxins known, are the causative agents of botulism, a lethal form of food poisoning. However, the importance of BoNTs has grown far beyond the estimated 250 annual cases of botulism. In recent years, BoNTs have become valuable treatments for a diverse array of conditions as severe as chronic pain, migraines, and cancer and as minor as tennis elbow and facial wrinkles. Perhaps most important, however, is the threat posed by those willing to use *botulinum* neurotoxins as weapons of bioterrorism [1–3]. The deliberate release of botulinum toxin into the nation's food or water supply could potentially result in hundreds of thousands of casualties [4]. A botulism outbreak of this magnitude would render the current treatments of BoNT intoxication inadequate.

Presently, treatment relies on antibodies capable of binding to and inhibiting BoNT endocytosis by neuronal cells. This requires knowledge of intoxication before the toxin is able to enter cells and cause symptoms, in most cases less than 24 hr. Thus, there is an urgent need for small-molecule inhibitors of *botulinum* toxins that target the toxin after it enters the cell.

Clostridium botulinum neurotoxin has been classified into seven antigenically unique serotypes (A–G), all of which are synthesized as a single protein of ~150 kDa (1295 residues) with three functional domains. After translation, the holotoxin is proteolyzed to yield the mature molecule, where the two polypeptide chains remain linked by a disulfide bond. The ~50 kDa light chain (LC; residues 1–448 of the holotoxin) is a Zn(II)-dependent endoprotease belonging to the thermolysin family of metalloproteases. The ~100 kDa heavy chain (HC) contains an N-terminal translocation domain (residues 449–872) and a C-terminal receptor-binding domain (residues 873–1295) [5–7].

BoNT intoxication has been described as a four-step process [8–11]. First, the toxin is ingested and enters the bloodstream, where the binding domain targets the protein to the presynaptic membrane of motor neurons. Next, BoNT enters the neuron by receptor-mediated endocytosis. Once in the acidic endosome, the translocation domain is believed to form a pore through which the light chain is released into the cytosol of the neuron. The last step is the LC-mediated proteolysis of specific proteins required for neurotransmitter release.

The toxicity of BoNTs results from the metalloprotease activity of the LC, which cleaves one of three soluble N-ethylmaleimide-sensitive factor attachment protein receptor (SNARE) proteins required for neuroexocytosis and release of acetylcholine. The blockade of acetylcholine release leads to the flaccid paralysis characteristic of BoNT intoxication. The specific SNARE protein targeted

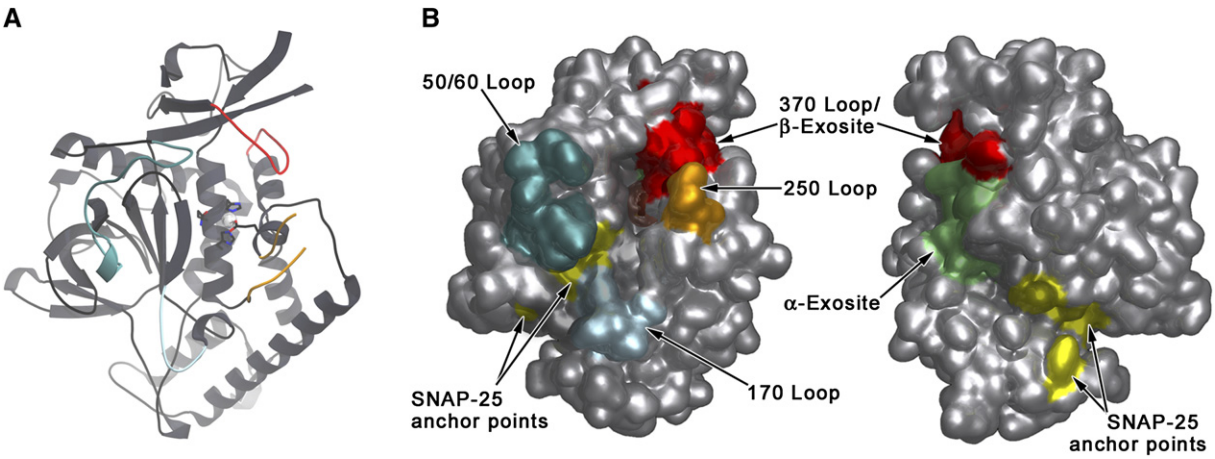

Figure 1. The Structure and Binding Sites of BoNT/A-LC

(A) Ribbon representation of the BoNT/A-LC(1–424) structure. The catalytic Zn(II) atom is shown as a metallic sphere. The four flexible active-site loops are highlighted in cyan (50/60 loop), light blue (170 loop), orange (250 loop), and red (370 loop).

(B) The surface of the protein shown in two orientations (related by a 180° rotation in Y) with the active-site loops colored as above. In addition, the α exosite is highlighted in green and the SNAP-25 "anchor points" described in [28] are colored yellow. The β exosite is comprised of residues from the 250 and 370 loops and thus, for clarity, is not highlighted with an additional color. This figure was rendered using POVScript+ [48, 49] and POVRAY (www.povray.org).

and the site of hydrolytic cleavage vary among the seven serotypes. BoNT/A, -E, and -C1 cleave synaptosome-associated protein of 25 kDa (SNAP-25), each at a unique peptide bond. BoNT/C also cleaves syntaxin. BoNT/B, -D, -F, and -G hydrolyze vesicle-associated membrane protein (VAMP; also known as synaptobrevin) [12–17]. These metalloproteases are unique in that they possess exquisite substrate specificity, requiring substrates with a minimum of ~40 residues for efficient cleavage [18–20].

As of this writing, crystal structures have been determined for six of the seven BoNT-LC serotypes (A, B, D, E, F, and G) [21–26]. The structures are all very similar (1.55 Å root-mean-square deviation [rmsd] for Cα atoms), as would be expected from the high sequence identity (~30%–60% among all seven serotypes) [27]. BoNT-LC is a roughly spherical, globular protein. At the center of the enzyme is a long α helix containing the HEXXH Zn(II)-binding motif that marks the active-site cleft. Four flexible loops, termed the 50/60 loop, 170 loop, 250 loop, and 370 loop (Figure 1), form the rim of the active-site cleft and presumably play a part in substrate binding. The remainder of the protein consists of mixed α/β structure. An extended, shallow trench runs from the active site to the opposite face of the protein (Figure 1). There is currently only one structure of a BoNT-SNARE protein complex [28]. The recently published structure of the complex of BoNT/A with the SNARE domain (residues 141–204) of SNAP-25 identified two exosites on the enzyme surface containing the bulk of the enzyme-substrate contacts [29]. It is clear that the interacting surfaces of BoNT/A and SNAP-25 are quite extensive, which would be expected to complicate the search for specific inhibitors of BoNT/A-LC metalloprotease activity.

Despite the apparent difficulties, however, a number of small-molecule inhibitors of BoNT-LCs have been identified [30–35], though none have yet been developed into drug therapies. Boldt et al. have recently developed a novel class of BoNT protease inhibitors with nanomolar affinity for the enzyme [36]. The initial lead, 4-chlorocinnamic hydroxamate (**1**; Figure 2) (IC_{50} = 15.0 μM), was obtained from a diverse library of hydroxamic acids. Subsequent structure-activity relationship (SAR) studies yielded the smallest, most potent BoNT inhibitor yet (K_i = 300.0 nM ± 12 nM), 2,4-dichlorocinnamic hydroxamate (**2**; Figure 2). Recently, **2** has been shown to have in vivo efficacy, with 16% of mice dosed (at 1 mM) surviving the BoNT challenge (~5–10 times the intraperitoneal LD_{50}) indefinitely with no obvious signs of botulism [37].

In order to determine the mode of action of this novel class of BoNT protease inhibitors, we determined the X-ray crystal structures of a C-terminal truncation mutant of the enzyme (residues 1–424) complexed with cinnamic hydroxamates **1** and **2** (LC:**1** and LC:**2**, respectively). Because BoNT/A cleaves SNAP-25 between residues Gln197 and Arg198, and because L-arginine hydroxamate is known to be a weak inhibitor of the toxin (IC_{50} = 60.0 μM), we also determined the structure of the complex of BoNT/A-LC with L-arginine hydroxamate (**3**; Figure 2) bound (LC:**3**). Recently, Fu et al. reported the structure of a different truncated form of BoNT/A-LC complexed with **3** [38] in which the protein contains two mutations (Y249F/Y250F) meant to prevent LC-catalyzed proteolysis of the 250 loop. We report a similar LC:**3** complex structure to provide a direct comparison to the LC:**1** and LC:**2** complex structures. Together, these structures provide several unexpected insights into the binding potential of the BoNT/A-LC active site. The structures also suggest ways to improve on the already potent inhibitor **2**.

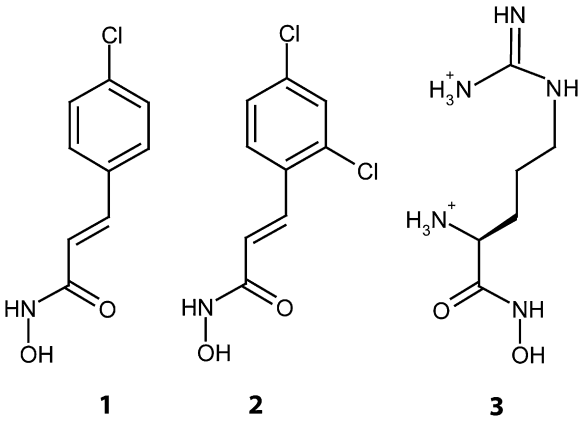

Figure 2. Chemical Structures of the Compounds Used in This Study

RESULTS AND DISCUSSION

The Native BoNT/A-LC(1–424) Structure

BoNT/A-LC(1–424) crystallized in space group $P2_1$ with two molecules in the asymmetric unit. The structure of this truncated form of the toxin was solved by molecular replacement using the model of another truncated form (residues 1–420; Protein Data Bank [PDB] ID code 1XTF) [28]. The truncated BoNT/A was derived from crystallization and kinetic trials to find the construct of maximal length that retained native activity and stability. The N-terminal His_6 tag was left intact after purification, and the sequence intervening between the polyhistidine tag and BoNT/A-LC (SSGLVPRGSH) is clearly visible in the electron density. The histidine immediately prior to Met1 was designated residue number zero. This N-terminal addition forms a portion of the dimer interface observed in the nonphysiological (crystallographic) dimer. The final model of native BoNT/A-LC includes residues −9 to 416. Several surface loops, including part of the 50/60 loop and the entire 250 loop, were disordered and, thus, omitted from the model.

The unliganded structure of truncated BoNT/A light chain (residues 1–424) was compared to the structure of the holotoxin light chain (PDB ID code 3BTA). Least-squares fitting in SSM [39] resulted in an rmsd for all α carbons common to both models of 0.92 Å. Visual inspection of the models shows that only the flexible loops surrounding the active site, two of which are disordered in the LC:**1**, LC:**2**, and LC:**3** structures (the 50/60 and 250 loops) and the C terminus, differ significantly between the two models (Figure 3). This indicates that the addition of the N-terminal His_6 tag and removal of the 24 C-terminal residues do not impact the structure of the LC. Because it is the full-length enzyme (residues 1–448) that would be targeted inside neurons, we had initially attempted our structural studies using the full-length LC (residues 1–448). These efforts proved unsuccessful. It is worth noting that every BoNT/A-LC structure published as of this writing uses some truncated form of the protein. Although it is likely that the C-terminal residues may form part of the

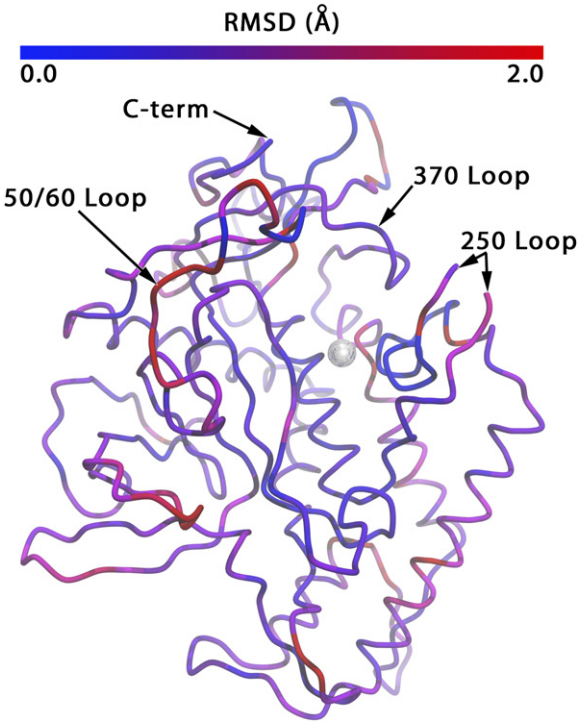

Figure 3. Comparison of Structures of BoNT/A-LC(1–424) and Holotoxin LC

The backbone of BoNT/A-LC(1–424) is shown as a Cα trace colored by the root-mean-square deviation of the Cα positions from those of the holotoxin LC structure (PDB ID code 3BTA). The scale runs from blue (rmsd of 0.0 Å) to red (rmsd of 2.0 Å). The overall rmsd value for the entire structure is 0.92 Å. Note that most of the structure, the active site in particular, is blue to purple. The regions having the largest differences between the two structures (red) are almost entirely confined to flexible loops on the surface of the protein. Two of the four active-site loops, the 50/60 loop and the 250 loop, show large deviations between the two structures. The catalytic Zn(II) ion (represented as a metallic sphere) marks the position of the active site. This figure was rendered using POVScript+ [48, 49] and POVRAY (www.povray.org).

active-site architecture, kinetic analysis of the full-length and truncated forms of the LC indicates that, while there are differences in the inhibition constants, compounds **1** and **2** are active against both forms of the metalloprotease (R.A. Fredenburg, personal communication).

The Perfect Fit

The three enzyme-inhibitor complex structures provide details about the interactions of the small-molecule inhibitors with the enzyme. As would be expected based on the similarity of compounds **1** and **2**, the inhibitors bind in almost identical orientations using the same set of interactions. Of particular interest is the comparison between the cinnamic hydroxamate inhibitors and L-arginine hydroxamate.

Both **1** and **2** bind with the cinnamyl side chain oriented toward the 370 loop, which forms a steep wall at one end of the active-site cleft and constitutes part of the β exosite described by Breidenbach and Brunger [28] (Figures 4A, 4B, 5A, and 5B). Due to the predominantly hydrophobic

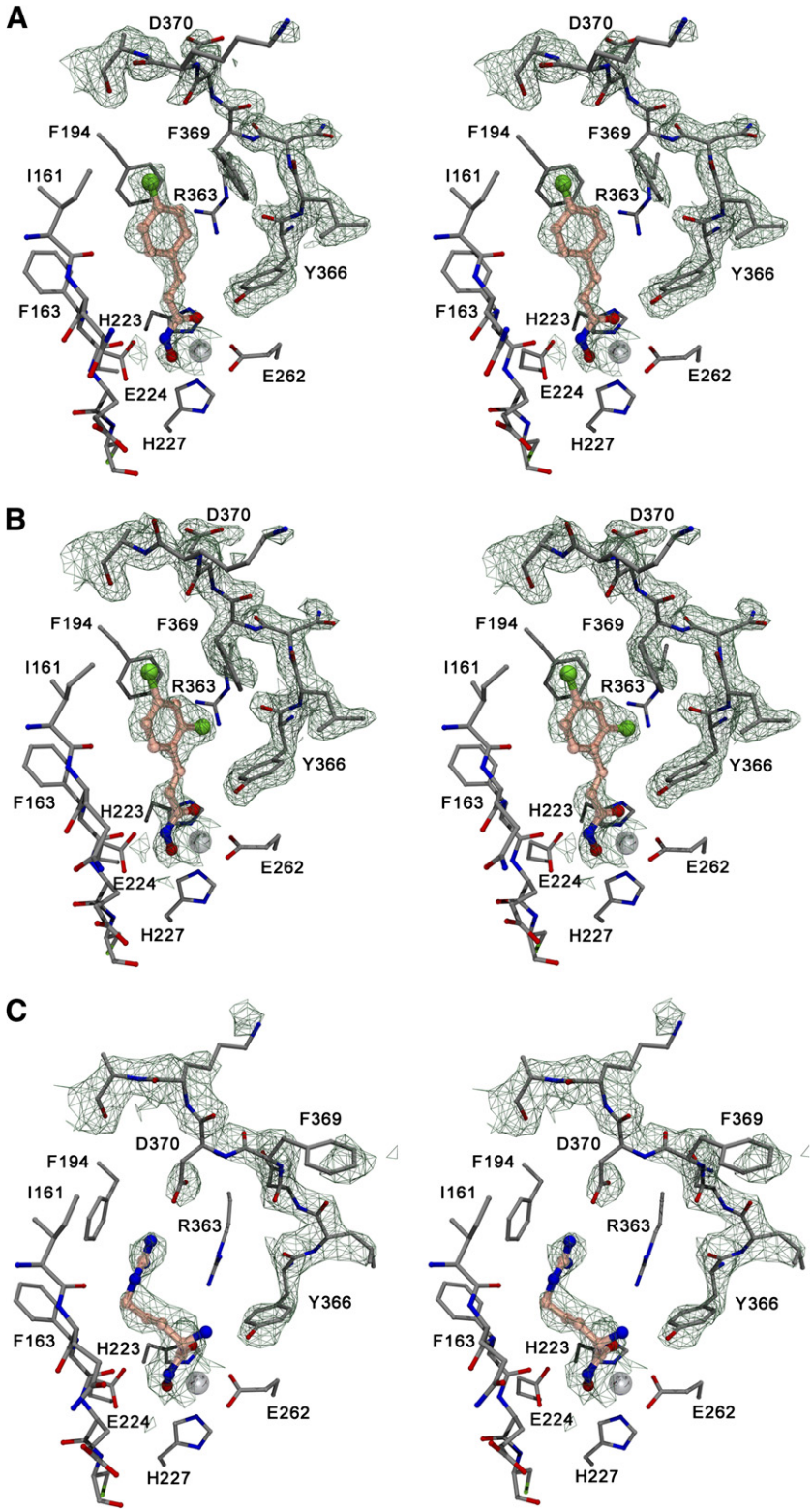

Figure 4. Structures of BoNT/A-LC(1–424) Bound to Hydroxamate Inhibitors

Stereo representations of the three enzyme-inhibitor complexes ([A], LC:**1**; [B], LC:**2**; [C], LC:**3**) showing the unweighted $2|F_o| - |F_c|$ simulated annealing composite omit electron-density maps (green mesh) for the inhibitor and residues 366–372 (the 370 loop) contoured at 1.25σ. Active-site residues are represented as cylinders with gray carbon atoms. The inhibitors are shown in ball-and-stick representation with brass carbons. The catalytic Zn(II) ions are rendered as metallic spheres. This figure was rendered using POVScript+ [48, 49] and POVRAY (www.povray.org).

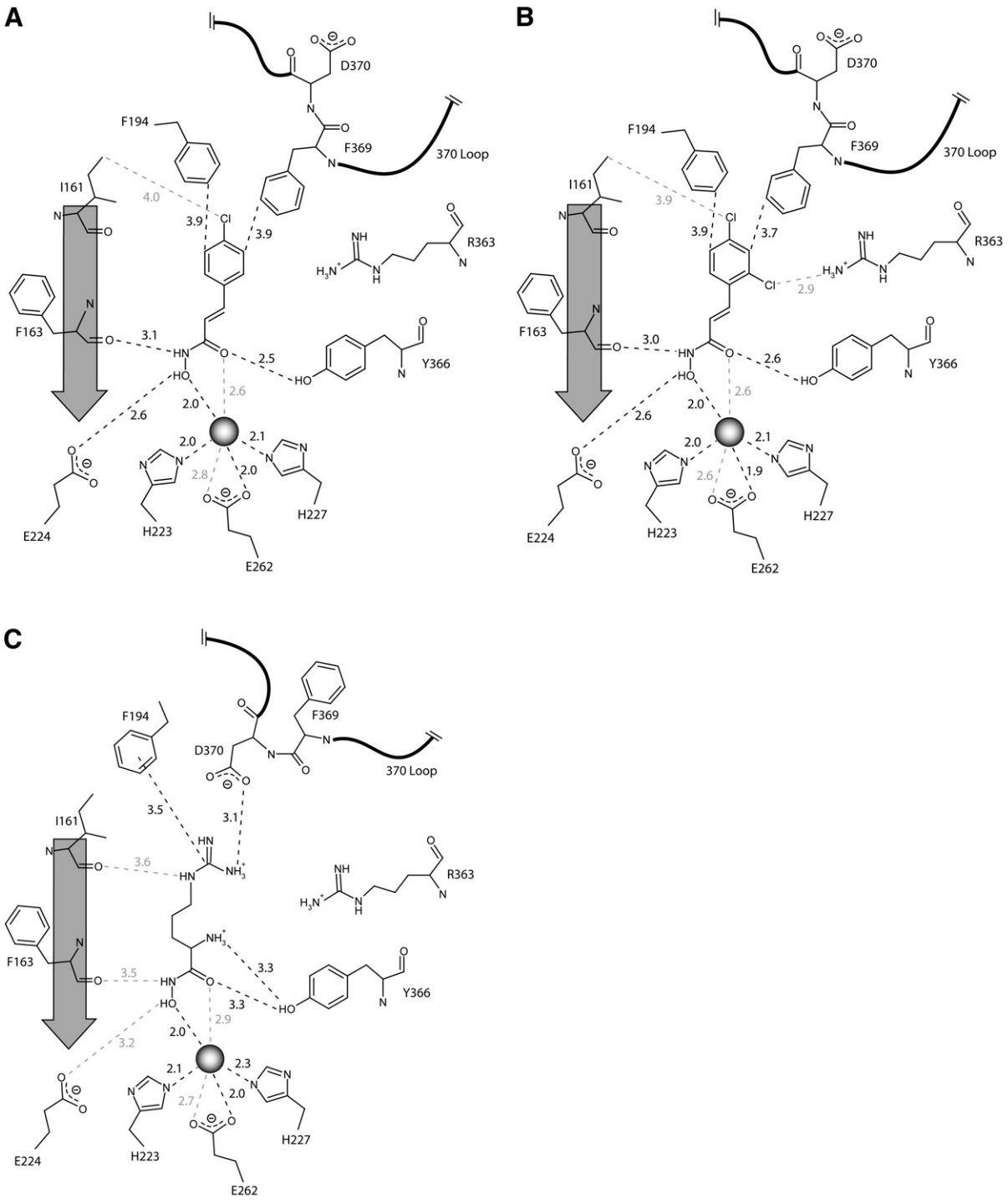

Figure 5. Schematic Representation of the Enzyme-Inhibitor Complexes

Hydrophobic interactions, metal ligands, and hydrogen bonds (distances in Å) are depicted for the complexes of **1** (A), **2** (B), and **3** (C) with BoNT/A-LC(1–424).

nature of **1** and **2**, there are very few hydrogen bonds formed between the inhibitors and functional groups in the enzyme active site. In both cases, the hydroxamate moiety has displaced the zinc-liganding water molecule observed in the native structure, and the hydroxyl oxygen of the hydroxamate moiety is coordinating the catalytic Zn(II) ion. Tyr366, one of two residues thought to stabilize the transition state during proteolysis [40], forms a hydrogen bond with the hydroxamate carbonyl oxygen. Glu224, part of the HEXXH motif typical of many zinc proteases,

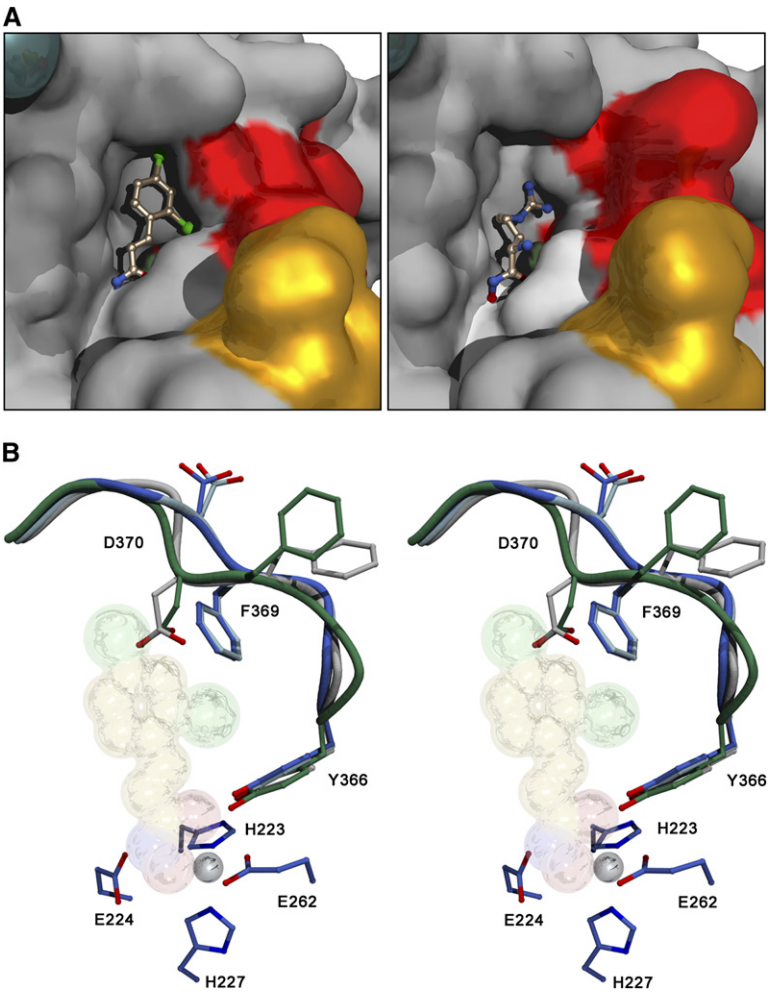

Figure 6. Conformational Changes in the Active Site of BoNT/A-LC(1–424)

(A) Surface representations showing the active sites of the LC:**2** (left) and LC:**3** (right) complexes. In both cases, the same active site conforms closely to the contours of both inhibitors. The 370 and 250 loops are colored red and orange, respectively.

(B) Stereo view showing an overlay of the 370 loop from the four structures: the BoNT/A-LC(1–424) unliganded structure (gray), LC:**1** complex (light blue), LC:**2** complex (dark blue), and LC:**3** complex (green). The HEXXH Zn(II)-binding motif of the LC:**2** complex and a transparent van der Waals surface of **2** are shown for reference. Note the dramatic rearrangement of residues Phe369 and Asp370. Both figures were prepared using POVScript+ [48, 49] and POVRAY (www.povray.org).

interacts with the hydroxyl oxygen of the hydroxamate. Finally, the hydroxamate amide nitrogen interacts with the backbone carbonyl oxygen of Phe163.

The catalytic cleft of BoNT/A-LC is unusual in that the residues lining the site are almost entirely hydrophobic. Although this observation is puzzling given the fact that this enzyme evolved to cleave a specific Gln-Arg peptide bond, it explains the strong preference for hydrophobic side chains exhibited by BoNT/A-LC in high-throughput screens [36]. The phenyl ring of the inhibitors binds in a tight pocket formed by Ile161, Phe194, and Phe369 (Figure 5). Inhibitors **1** and **2** both completely fill the pocket as though it were tailored to these molecules (Figure 6A). The complementary shape of the active site explains the results of the SAR studies on **1** [36], which showed that substitution of the *p*-chloro group with a large *t*-butyl group leads to a dramatic decrease in potency. Similarly, addition of a *meta*-chloro group significantly reduced potency. One can see from Figure 6A that any group in the *meta* position would clash with the 370 loop. Conversely, addition of the *ortho*-chloro substituent to **1** (compound **2**) led to a 36-fold increase in potency, as the additional chlorine atom fills the void seen in the LC:**1** structure (Figure 6A).

An Equal-Opportunity Active Site

A surprising finding was made when the LC:**1** and LC:**2** structures were compared to the LC:**3** structure. The catalytic center, including the HEXXH motif, the catalytic Zn(II) ion, and the Glu262 zinc-binding residue, is identical across the three complex structures. The hydroxamate of **3** makes the same interactions with the enzyme described for **1** and **2** above. However, there is a dramatic difference in the overall shape and charge of the active site. The catalytic cleft has undergone a rearrangement to bind the Arg side chain of **3** (Figures 6A and 6B). The 370 loop takes on a different conformation from that seen in the complexes with the cinnamic hydroxamates. The side chain of Phe369 is withdrawn from the catalytic cleft and in its place is the carboxylate of Asp370, in position to participate in a salt bridge with the guanidinium group of **3**. The guanidinium group is also positioned to form a π cation bond with the face of the phenyl ring of Phe194. Finally, the carbonyl oxygen of Ile161 is close enough (3.6 Å) to the guanidinium group of **3** to form a hydrogen bonding interaction (Figure 5C). Far from forming a rigid wall of the active site, the 370 loop is capable of dramatic rearrangements in response to the electrostatic character of the substrate. Thus, BoNT/A-LC displays a localized form of

Table 1. Data Collection and Refinement Statistics

	LC	LC:**1**	LC:**2**	LC:**3**
Resolution (Å) (last shell)[a]	50.0–2.00 (2.07–2.00)	50.0–1.94 (2.01–1.94)	50.0–1.90 (1.97–1.90)	50.0–2.50 (2.59–2.50)
Wavelength (Å)	1.0720	1.0000	1.0000	1.1000
Space group	$P2_1$	$P2_1$	$P2_1$	$P2_1$
Cell dimensions (Å)	a = 73.2, b = 67.5, c = 97.7, β = 106.5	a = 73.4, b = 67.3, c = 98.1, β = 106.5	a = 73.8, b = 67.7, c = 98.5, β = 106.6	a = 72.5, b = 67.2, c = 96.9, β = 104.7
Reflections				
Observed	188,216	159,950	249,622	112,375
Unique	60,496	63,852	71,771	32,735
Completeness (%)[a]	95.6 (79.8)	93.7 (96.3)	97.9 (95.3)	99.3 (99.6)
R_{merge} (%)[a,b]	7.2 (38.7)	7.4 (57.8)	9.4 (45.5)	14.3 (51.2)
$I/\sigma(I)$[a]	11.5 (2.8)	9.0 (2.1)	12.3 (3.2)	9.2 (2.8)
Refinement Statistics				
Number of protein/water atoms per asymmetric unit	6,508/426	6,604/621	6,519/467	6,466/275
Number of reflections (work/free)	57,400/3,078	68,126/3,626	60,589/3,232	33,688/1,778
R_{work}/R_{free} (%)	19.0/23.2	18.6/23.1	19.8/24.7	19.6/26.9
Average B factor (Å^2)				
Protein atoms	32.3	33.8	34.3	29.0
Inhibitor	na	41.1	49.8	44.4
Zn(II) ions	24.6	24.6	28.4	26.6
Water	39.2	39.5	41.3	31.5
Rms deviations				
Bond lengths (Å)	0.024	0.009	0.010	0.016
Bond angles (°)	1.765	1.151	1.233	1.552

na, not applicable.
[a] Values in parentheses apply to the high-resolution shell indicated in the resolution row.
[b] $R = \Sigma(I - \langle I \rangle)^2/\Sigma I^2$.

the induced-fit model of substrate specificity that could be termed "substrate switching."

In BoNT/A, it has been suggested that Phe162, Thr192, and Thr219 may form the S1′ subsite responsible for binding the P1′ arginine side chain of SNAP-25 [41]. The structures reported here as well as the structure of BoNT/A-LC(1–420) bound to SNAP-25 [28] suggest that the S1′ subsite is instead formed by residues Phe194, Ile161, and Asp370. This interpretation is supported, at least in part, by the recently published structure of a similar truncated form of BoNT/A-LC with L-arginine hydroxamate bound [38].

The plasticity of the BoNT/A-LC active site and the apparent lack of substrate-specificity pockets other than the S1′ subsite suggest that the BoNT proteases derive their exquisite substrate specificity almost entirely from the α and β exosites. This concept is supported by the ability of the LC to catalyze autoproteolytic cleavage of the 250 loop at the Tyr250-Tyr251 bond. Segelke et al. [42] observed the "product complex" of this cleavage, wherein the main chain of the cleaved 250 loop is oriented in the opposite direction of SNAP-25 binding. Thus, the substrate switching observed herein explains both the specificity for the QRATKML motif of SNAP-25 and the autoproteolytic activity at a hydrophobic loop.

SIGNIFICANCE

The structures of BoNT/A-LC(1–424) in complexes with 4-chlorocinnamic hydroxamate (1) or 2,4-dichlorocinnamic hydroxamate (2) provide detailed information about the binding mode of these BoNT protease inhibitors. Because 2 is the most potent BoNT/A-LC inhibitor yet discovered, and has been shown to possess in vivo activity in mice prechallenged with BoNT [37], the LC:2 structure will be valuable in the design of more potent and selective compounds. Taken together, the three complex structures demonstrate the remarkable plasticity of specificity of this enzyme for small molecules. The catalytic center itself has

little or no built-in selectivity for substrate residues other than the P1′ arginine. This is remarkable because the BoNT proteases are among the most specific proteases known. It would appear that BoNT/A, if not the other BoNT serotypes, relies on the α and β exosites for substrate specificity. The highly plastic active site observed here, capable of accommodating molecules of varying shape, size, and charge, may be exploited for drug design. While it would initially seem that this plasticity should hinder efforts to design specific inhibitors of this enzyme, the reverse may be true. The adaptability of the BoNT/A active site could make it possible not only to target the catalytic Zn(II) ion but also stabilize the catalytic pocket in a conformation that is not competent for proteolysis of SNARE complex proteins.

EXPERIMENTAL PROCEDURES

Cloning, Expression, and Purification

The cDNA encoding the full-length (1–448) BoNT/A-LC gene was synthesized by Midland Certified Reagent Company (Midland, TX). Oligonucleotide primers (5′-GGAATTCCATATGCCATTTGTTAATAAACAATTTAATT-3′ and 5′-CGGGATCCTTATTCAAACAATCCAGTAAAAT-3′), containing cleavage sites for the restriction endonucleases NdeI and BamHI (underlined), were used to amplify the BoNT/A-LC(1–424) open reading frame. The BoNT/A-LC(1–424) gene was cloned into the pET-15b(+) vector (Stratagene, La Jolla, CA). The ligation product (pET-15b[+]-BoNT/A-LC[1–424]) was used to transform *Escherichia coli* DH5α competent cells. The purified plasmid was sequenced by the Tufts University Core Facility.

BoNT/A-LC(1–424) was purified from *E. coli* BL21 (DE3)-gold cells (Stratagene) containing the pET-15b(+)-BoNT/A-LC(1–424) plasmid as follows. Transformed cells were grown at 30°C in Luria broth containing 50 μg/ml ampicillin. When the OD_{600} of the culture reached 0.6–1.0, the temperature was reduced to 18°C, and the cultures were induced overnight with 0.5 mM isopropyl-β-D-thiogalactopyranoside (IPTG). Cells were harvested by centrifugation, and the pellet was suspended in 100 ml of lysis buffer (20 mM HEPES [pH 8.0], 500 mM NaCl, 10 mM imidazole, 1 mM phenylmethylsulfonyl fluoride [PMSF]).

The cells were lysed using a microfluidizer, and the N-terminally His_6-tagged protein was purified by immobilized metal ion-affinity chromatography using HiTrap chelating resin (GE Healthcare Biosciences AB, Uppsala, Sweden) charged with Zn(II). The protein was eluted in 20 mM HEPES (pH 8.0), 500 mM NaCl, 250 mM imidazole and was estimated to be >95% pure by SDS-PAGE. The purified BoNT/A-LC(1–424) was desalted by dialysis against 8 liters of 20 mM HEPES (pH 7.5), 50 mM NaCl. Finally, the purified, desalted enzyme was concentrated to ~10 mg/ml using Amicon centrifugal concentrators (Millipore, Billerica, MA) having a nominal molecular weight cutoff of 10 kDa.

Crystallization and Data Collection

Crystals of the unliganded, truncated BoNT/A-LC were obtained by the hanging drop vapor diffusion method. Drops were formed of equal parts BoNT/A-LC(1–424) at 10 mg/ml in 20 mM HEPES (pH 7.5), 50 mM NaCl and well solution containing 10%–15% polyethylene glycol monomethyl ether 2000 (PEG-2K MMe), 0.3 M $(NH_4)_2HPO_4$, 50 mM Tris (pH 8.5). Compound **2** was cocrystallized with the enzyme by adding 500 μM **2** to the protein solution. Small (0.1 × 0.02 × <0.01 mm), plate-like crystals grew in 1–3 days. Larger crystals were obtained by microseeding.

X-ray diffraction data were collected at the National Synchrotron Light Source, beamline X12B. The LC:**1** structure was obtained by soaking crystals of the unliganded enzyme for 7 min in a solution of 20% PEG-2K MMe, 0.3 M $(NH_4)_2HPO_4$, 50 mM Tris (pH 8.5), 20% glycerol, and 5 mM **1**. The soaked crystal (0.4 × 0.05 × ~0.01 mm) was flash-cooled to 100K in a gaseous N_2 stream and data were collected to 1.90 Å. For the LC:**2** complex, data were collected from a BoNT/A-LC(1–424) cocrystal (vide supra). The 0.5 × 0.1 × ~0.02 mm crystal was transferred in three steps (5%, 10%, and 20% glycerol) to a solution of 20% PEG-2K MMe, 0.3 M $(NH_4)_2HPO_4$, 50 mM Tris (pH 8.5), 20% glycerol and flash-cooled to 100K. The complex of the enzyme with L-arginine hydroxamate was obtained by soaking a 0.4 × 0.1 × 0.01 mm crystal of the unliganded enzyme for 60 hr in 20% PEG-2K MMe, 0.3 M $(NH_4)_2HPO_4$, 50 mM Tris (pH 8.5), 20% glycerol, and 50 mM **3**. Data were collected at 100K. Finally, data were collected on a crystal of the unliganded enzyme for comparison to the three enzyme-inhibitor complexes. All four data sets were indexed and scaled using DENZO and SCALEPACK [43]. Data collection statistics for all four data sets can be found in Table 1.

Structure Determination and Model Refinement

The structure of the unliganded BoNT/A-LC(1–424) was solved by molecular replacement using the structure of a mutant form of BoNT/A-LC containing residues 1–420 (PDB ID code 1XTF) as the search model. Repeating the molecular replacement using other BoNT/A-LC structures (PDB ID codes 1E1H and 3BTA) resulted in a nearly identical model of BoNT/A-LC(1–424) after several rounds of refinement (data not shown). Molecular replacement was performed with PHASER [44]. The three enzyme-inhibitor complex structures were each phased by difference Fourier methods using phases from the unliganded BoNT/A-LC(1–424) model.

All four models were refined using REFMAC5 [45]. The same general refinement protocol was used for all four models. Briefly, after one round of rigid body refinement, individual atomic coordinates and isotropic temperature factors were refined. Next, water molecules visible as spherical peaks in $|F_o| - |F_c|$ electron-density maps contoured at 3.0σ were added to the models. Missing sections of the model were built by an iterative process of model building in Coot [46] and refinement in REFMAC5. Once the R factors converged, the inhibitor molecules were built into $|F_o| - |F_c|$ electron density. No noncrystallographic symmetry restraints were used because they did not improve the phases significantly. The models were finished by making changes suggested by validation tools in Coot and MOLPROBITY [47]. Refinement statistics for the four models are given in Table 1.

ACKNOWLEDGMENTS

This work was supported by contract NO1-AI30050 from the National Institutes of Health (NIH) and the National Institute of Allergy and Infectious Diseases (NIAID) as well as NIH training grant HL07291 (to N.R.S.).

Received: October 5, 2006
Revised: February 7, 2007
Accepted: March 14, 2007
Published: May 29, 2007

REFERENCES

1. Hanson, D. (2004). Botulinum toxin: a bioterrorism weapon. Emerg. Med. Serv. *33*, 55–59.
2. Josko, D. (2004). Botulin toxin: a weapon in terrorism. Clin. Lab. Sci. *17*, 30–34.
3. Patocka, J., Splino, M., and Merka, V. (2005). Botulism and bioterrorism: how serious is this problem? Acta Medica (Hradec Kralove) *48*, 23–28.
4. Wein, L.M., and Liu, Y. (2005). Analyzing a bioterror attack on the food supply: the case of botulinum toxin in milk. Proc. Natl. Acad. Sci. USA *102*, 9984–9989.

5. Montecucco, C., and Schiavo, G. (1995). Structure and function of tetanus and botulinum neurotoxins. Q. Rev. Biophys. *28*, 423–472.
6. Krieglstein, K.G., DasGupta, B.R., and Henschen, A.H. (1994). Covalent structure of botulinum neurotoxin type A: location of sulfhydryl groups, and disulfide bridges and identification of C-termini of light and heavy chains. J. Protein Chem. *13*, 49–57.
7. Sagane, Y., Watanabe, T., Kouguchi, H., Sunagawa, H., Inoue, K., Fujinaga, Y., Oguma, K., and Ohyama, T. (1999). Dichain structure of botulinum neurotoxin: identification of cleavage sites in types C, D, and F neurotoxin molecules. J. Protein Chem. *18*, 885–892.
8. Finkelstein, A. (1990). Channels formed in phospholipid bilayer membranes by diphtheria, tetanus, botulinum and anthrax toxin. J. Physiol. (Paris) *84*, 188–190.
9. Hambleton, P. (1994). Botulinum toxin: structure and pharmacology. Eur. Arch. Otorhinolaryngol. (*Suppl*), S200–S202.
10. Montecucco, C., and Schiavo, G. (1994). Mechanism of action of tetanus and botulinum neurotoxins. Mol. Microbiol. *13*, 1–8.
11. Montecucco, C., Schiavo, G., and Rossetto, O. (1996). The mechanism of action of tetanus and botulinum neurotoxins. Arch. Toxicol. Suppl. *18*, 342–354.
12. Yamasaki, S., Binz, T., Hayashi, T., Szabo, E., Yamasaki, N., Eklund, M., Jahn, R., and Niemann, H. (1994). Botulinum neurotoxin type G proteolyses the Ala81-Ala82 bond of rat synaptobrevin 2. Biochem. Biophys. Res. Commun. *200*, 829–835.
13. Yamasaki, S., Hu, Y., Binz, T., Kalkuhl, A., Kurazono, H., Tamura, T., Jahn, R., Kandel, E., and Niemann, H. (1994). Synaptobrevin/vesicle-associated membrane protein (VAMP) of *Aplysia californica*: structure and proteolysis by tetanus toxin and botulinal neurotoxins type D and F. Proc. Natl. Acad. Sci. USA *91*, 4688–4692.
14. Schiavo, G., Benfenati, F., Poulain, B., Rossetto, O., Polverino de Laureto, P., DasGupta, B.R., and Montecucco, C. (1992). Tetanus and botulinum-B neurotoxins block neurotransmitter release by proteolytic cleavage of synaptobrevin. Nature *359*, 832–835.
15. Binz, T., Blasi, J., Yamasaki, S., Baumeister, A., Link, E., Sudhof, T.C., Jahn, R., and Niemann, H. (1994). Proteolysis of SNAP-25 by types E and A botulinal neurotoxins. J. Biol. Chem. *269*, 1617–1620.
16. Blasi, J., Chapman, E.R., Yamasaki, S., Binz, T., Niemann, H., and Jahn, R. (1993). Botulinum neurotoxin C1 blocks neurotransmitter release by means of cleaving HPC-1/syntaxin. EMBO J. *12*, 4821–4828.
17. Blasi, J., Chapman, E.R., Link, E., Binz, T., Yamasaki, S., De Camilli, P., Sudhof, T.C., Niemann, H., and Jahn, R. (1993). Botulinum neurotoxin A selectively cleaves the synaptic protein SNAP-25. Nature *365*, 160–163.
18. Washbourne, P., Pellizzari, R., Baldini, G., Wilson, M.C., and Montecucco, C. (1997). Botulinum neurotoxin types A and E require the SNARE motif in SNAP-25 for proteolysis. FEBS Lett. *418*, 1–5.
19. Schmidt, J.J., and Bostian, K.A. (1995). Proteolysis of synthetic peptides by type A botulinum neurotoxin. J. Protein Chem. *14*, 703–708.
20. Yamasaki, S., Baumeister, A., Binz, T., Blasi, J., Link, E., Cornille, F., Roques, B., Fykse, E.M., Sudhof, T.C., Jahn, R., et al. (1994). Cleavage of members of the synaptobrevin/VAMP family by types D and F botulinal neurotoxins and tetanus toxin. J. Biol. Chem. *269*, 12764–12772.
21. Arndt, J.W., Chai, Q., Christian, T., and Stevens, R.C. (2006). Structure of botulinum neurotoxin type D light chain at 1.65 Å resolution: repercussions for VAMP-2 substrate specificity. Biochemistry *45*, 3255–3262.
22. Arndt, J.W., Yu, W., Bi, F., and Stevens, R.C. (2005). Crystal structure of botulinum neurotoxin type G light chain: serotype divergence in substrate recognition. Biochemistry *44*, 9574–9580.
23. Agarwal, R., Eswaramoorthy, S., Kumaran, D., Binz, T., and Swaminathan, S. (2004). Structural analysis of botulinum neurotoxin type E catalytic domain and its mutant Glu212→Gln reveals the pivotal role of the Glu212 carboxylate in the catalytic pathway. Biochemistry *43*, 6637–6644.
24. Swaminathan, S., and Eswaramoorthy, S. (2000). Structural analysis of the catalytic and binding sites of *Clostridium botulinum* neurotoxin B. Nat. Struct. Biol. *7*, 693–699.
25. Lacy, D.B., Tepp, W., Cohen, A.C., DasGupta, B.R., and Stevens, R.C. (1998). Crystal structure of botulinum neurotoxin type A and implications for toxicity. Nat. Struct. Biol. *5*, 898–902.
26. Agarwal, R., Binz, T., and Swaminathan, S. (2005). Structural analysis of botulinum neurotoxin serotype F light chain: implications on substrate binding and inhibitor design. Biochemistry *44*, 11758–11765.
27. Lacy, D.B., and Stevens, R.C. (1999). Sequence homology and structural analysis of the clostridial neurotoxins. J. Mol. Biol. *291*, 1091–1104.
28. Breidenbach, M.A., and Brunger, A.T. (2004). Substrate recognition strategy for botulinum neurotoxin serotype A. Nature *432*, 925–929.
29. Breidenbach, M.A., and Brunger, A.T. (2005). New insights into clostridial neurotoxin-SNARE interactions. Trends Mol. Med. *11*, 377–381.
30. Anne, C., Turcaud, S., Quancard, J., Teffo, F., Meudal, H., Fournie-Zaluski, M.C., and Roques, B.P. (2003). Development of potent inhibitors of botulinum neurotoxin type B. J. Med. Chem. *46*, 4648–4656.
31. Blommaert, A., Turcaud, S., Anne, C., and Roques, B.P. (2004). Small tripeptide surrogates with low nanomolar affinity as potent inhibitors of the botulinum neurotoxin B metallo-proteolytic activity. Bioorg. Med. Chem. *12*, 3055–3062.
32. Burnett, J.C., Schmidt, J.J., Stafford, R.G., Panchal, R.G., Nguyen, T.L., Hermone, A.R., Vennerstrom, J.L., McGrath, C.F., Lane, D.J., Sausville, E.A., et al. (2003). Novel small molecule inhibitors of botulinum neurotoxin A metalloprotease activity. Biochem. Biophys. Res. Commun. *310*, 84–93.
33. Schmidt, J.J., and Stafford, R.G. (2002). A high-affinity competitive inhibitor of type A botulinum neurotoxin protease activity. FEBS Lett. *532*, 423–426.
34. Schmidt, J.J., and Stafford, R.G. (2005). Botulinum neurotoxin serotype F: identification of substrate recognition requirements and development of inhibitors with low nanomolar affinity. Biochemistry *44*, 4067–4073.
35. Park, J.G., Sill, P.C., Makiyi, E.F., Garcia-Sosa, A.T., Millard, C.B., Schmidt, J.J., and Pang, Y.P. (2006). Serotype-selective, small-molecule inhibitors of the zinc endopeptidase of botulinum neurotoxin serotype A. Bioorg. Med. Chem. *14*, 395–408.
36. Boldt, G.E., Kennedy, J.P., and Janda, K.D. (2006). Identification of a potent botulinum neurotoxin A protease inhibitor using in situ lead identification chemistry. Org. Lett. *8*, 1729–1732.
37. Eubanks, L.M., Hixon, M.S., Jin, W., Hong, S., Clancy, C.M., Tepp, W.H., Baldwin, M.R., Malizio, C.J., Goodnough, M.C., Barbieri, J.T., et al. (2007). An in vitro and in vivo disconnect uncovered through high-throughput identification of botulinum neurotoxin A antagonists. Proc. Natl. Acad. Sci. USA *104*, 2602–2607.
38. Fu, Z., Chen, S., Baldwin, M.R., Boldt, G.E., Crawford, A., Janda, K.D., Barbieri, J.T., and Kim, J.J. (2006). Light chain of botulinum neurotoxin serotype A: structural resolution of a catalytic intermediate. Biochemistry *45*, 8903–8911.
39. Krissinel, E., and Henrick, K. (2004). Secondary-structure matching (SSM), a new tool for fast protein structure alignment in three dimensions. Acta Crystallogr. D Biol. Crystallogr. *60*, 2256–2268.

40. Binz, T., Bade, S., Rummel, A., Kollewe, A., and Alves, J. (2002). Arg(362) and Tyr(365) of the botulinum neurotoxin type A light chain are involved in transition state stabilization. Biochemistry *41*, 1717–1723.

41. Agarwal, R., Binz, T., and Swaminathan, S. (2005). Analysis of active site residues of botulinum neurotoxin E by mutational, functional, and structural studies: Glu335Gln is an apoenzyme. Biochemistry *44*, 8291–8302.

42. Segelke, B., Knapp, M., Kadkhodayan, S., Balhorn, R., and Rupp, B. (2004). Crystal structure of *Clostridium botulinum* neurotoxin protease in a product-bound state: evidence for noncanonical zinc protease activity. Proc. Natl. Acad. Sci. USA *101*, 6888–6893.

43. Otwinowski, Z., and Minor, W. (1997). Processing of X-ray diffraction data collected in oscillation mode. Methods Enzymol. *276*, 307–326.

44. CCP4 (Collaborative Computational Project, Number 4) (1994). The CCP4 suite: programs for protein crystallography. Acta Crystallogr. D Biol. Crystallogr. *50*, 760–763.

45. Murshudov, G.N., Vagin, A.A., and Dodson, E.J. (1997). Refinement of macromolecular structures by the maximum-likelihood method. Acta Crystallogr. D Biol. Crystallogr. *53*, 240–255.

46. Emsley, P., and Cowtan, K. (2004). Coot: model-building tools for molecular graphics. Acta Crystallogr. D Biol. Crystallogr. *60*, 2126–2132.

47. Davis, I.W., Murray, L.W., Richardson, J.S., and Richardson, D.C. (2004). MOLPROBITY: structure validation and all-atom contact analysis for nucleic acids and their complexes. Nucleic Acids Res. *32*, W615–W619.

48. Kraulis, P. (1991). MOLSCRIPT: a program to produce both detailed and schematic plots of protein structures. J. Appl. Cryst. *24*, 946–950.

49. Fenn, T.D., Ringe, D., and Petsko, G.A. (2003). POVScript+: a program for model and data visualization using persistence of vision ray-tracing. J. Appl. Cryst. *36*, 944–947.

Accession Numbers

Coordinates and structure factors for *C. botulinum* neurotoxin serotype A light chain in the unliganded form and bound to 4-chlorocinnamic hydroxamate, 2,4-dichlorocinnamic hydroxamate, and L-arginine hydroxamate have been deposited in the Protein Data Bank under ID codes 2IMC, 2ILP, 2IMA, and 2IMB, respectively.

